An intrinsically safe facility for forefront research and training on nuclear technologies -- Core Design

C. M. Viberti
G. Ricco
I.N.F.N. Genova - University of Genova

Abstract

The core of a subcritical, low-power research reactor in a lead matrix has been designed using the MCNPX code. The main parameters, like geometry, material composition in the fuel assembly and reflector size, have been optimized for a k_{eff}~0.95 and a thermal power around 200 Kw. A 70 Mev, 1 mA proton beam incident on a beryllium target has been assumed as neutron source and the corresponding thermal power distribution and neutron fluxes in the reactor have been simulated.

2.1 Reactor Core Optimization.

Geometry and material composition of the *fuel assembly (FA)*, which is shown in Figure 2.1, are the main constraints for the starting point in the study of the reactor core. In the figure, it is shown the Lead array (yellow) in which are inserted 9x9 fuel rods, composed of UO_2 with Uranium *20%* enriched in the isotope ^{235}U (red) and fuel cladding made of *AISI304L* (light blue): the fuel pin diameter is *7.14 mm* and the fuel cladding thickness is *0.68 mm*. Cooling Helium gas flows in *2.50 mm* channels (pink); each channel is conservatively coated by an Aluminum tube *0.50 mm* thick (violet). The rigid stainless steel container *AISI304* (green) and the empty space between the *FAs* (white) are respectively *2.00 mm* and *0.70 mm* thick. Each single *FA*, with a total height and an active length of *130 cm* and *90 cm* respectively, contains around *30 kg* of UO_2 and *45 kg* of Lead, which are the major abundant constituents.
Further constraints are given by the number and arrangement of the *FAs* and the thickness of the surrounding Lead reflector, designed to form a system with cylindrical symmetry (Figure 2.2) so that $k_{eff} \cong 0.95$ and $P < 500$ *kW*. In Figure 2.3, the reflector thickness (*i.e.* the external radius of the lateral reflector) is plotted against the total number of *FAs*, for some reasonable configurations: the configuration chosen minimizes the total number of *FAs* (thus reducing costs without increasing excessively the structure weight), while maintaining an approximate value of *0.95* for k_{eff}. Simulations were done using *MCNPX v. 2.6.0* [1] with *ENDF/B.-VII* database [2]. With this configuration, it is possible to obtain $k_{eff} = 0.95$ with cylindrical geometry; increasing further the extension of the reflector (over *120 cm* radius) would lead to

a small increase of k_{eff} but a significant increase in weight and manufacturing costs. For the same reason, also axial reflectors were fixed at the saturation value (*30 cm*).
This "optimized"-configuration is drown to-scale in Figure 2.4, and is composed of *60 FAs* arranged in cylindrical symmetry and surrounded by *75 cm* of Lead; the reactor total radial extension is *122 cm*, including *2 cm* of stainless steel vessel. The system is mainly composed of about *2 tons* of fuel and *87 tons* of Lead (around *3 tons* into fuel assemblies).

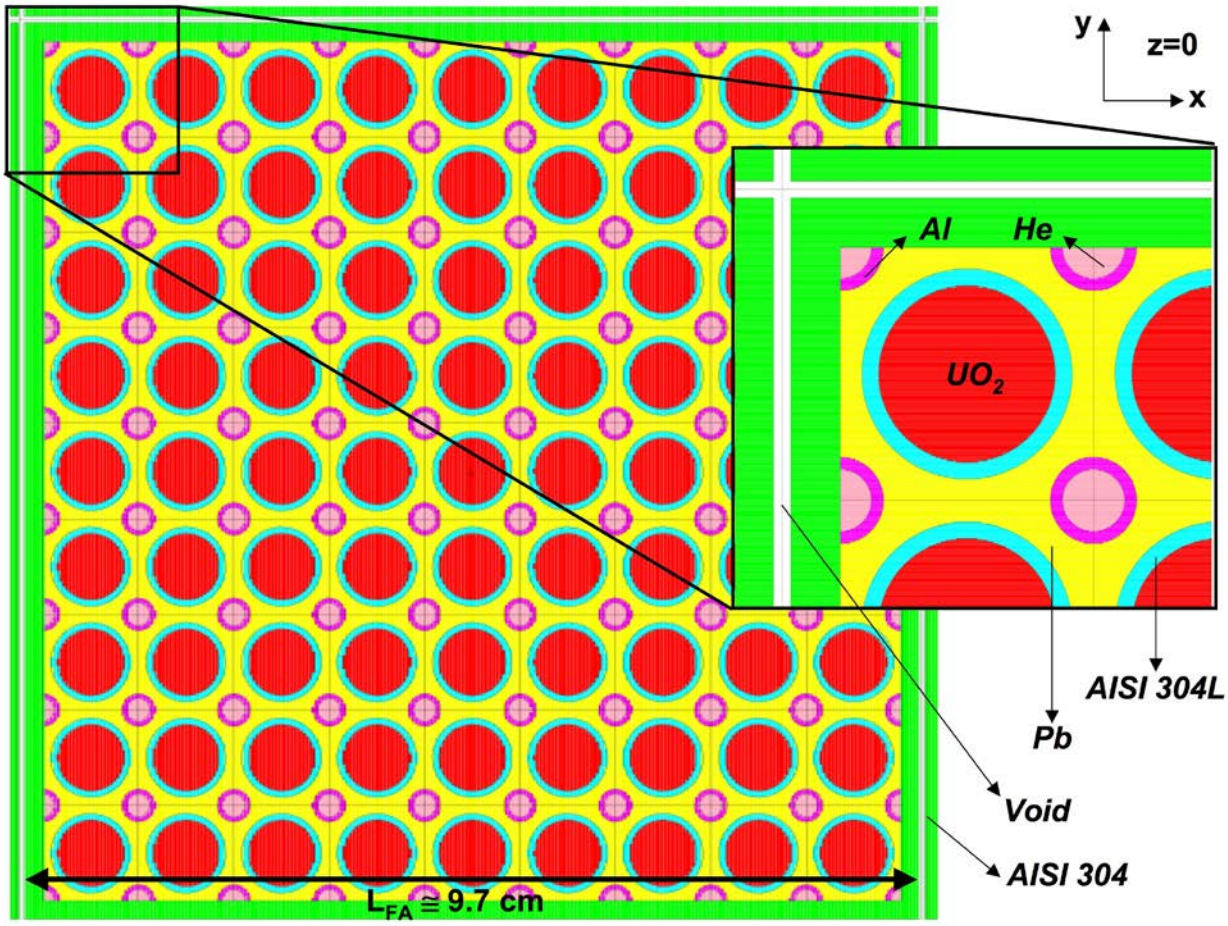

Figure 2.1 *FA* cross-sectional area with *9x9* fuel rods. Dimensions are not inserted for not weight the picture.

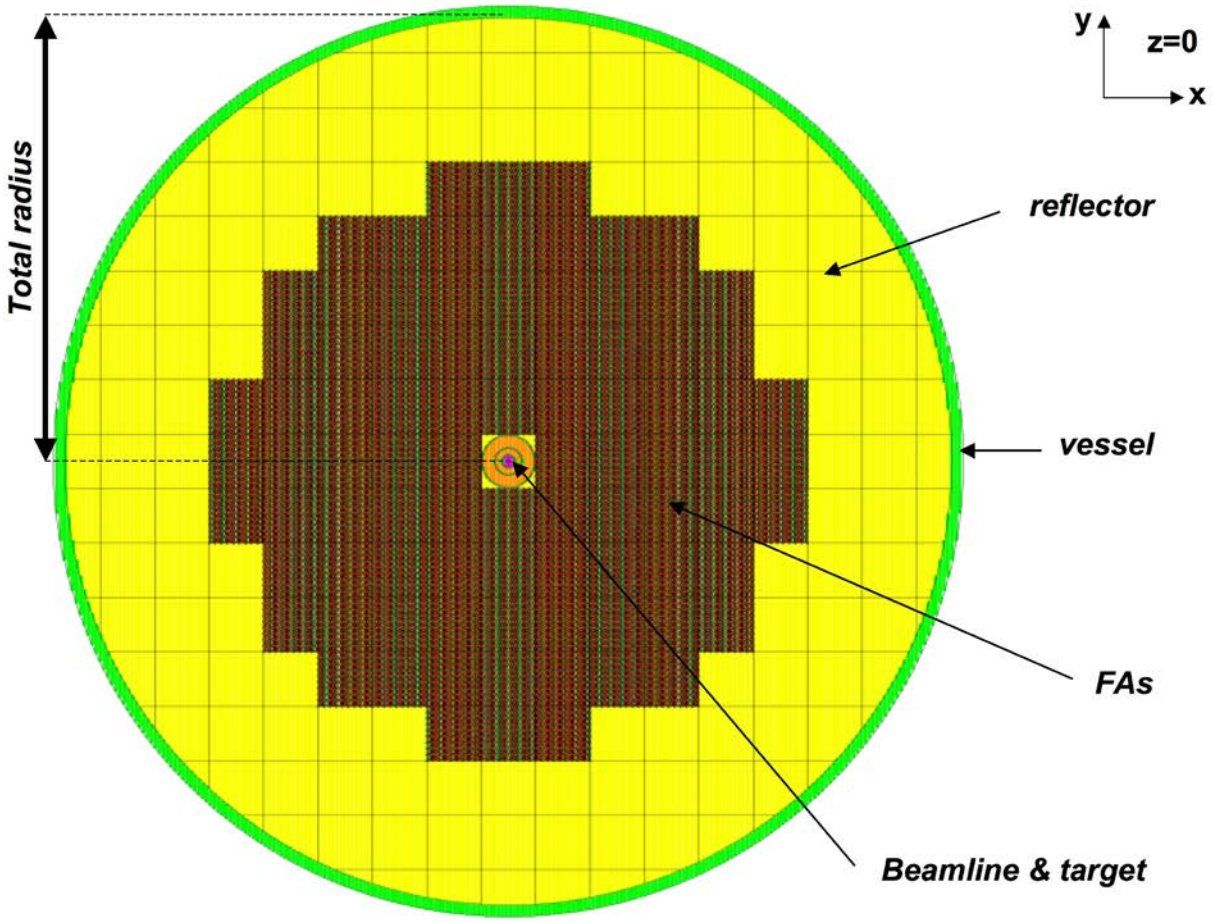

Figure 2.2 Reactor cross-sectional area: *FAs* form a cylindrical symmetry configuration around the beam-line, the core is surrounded by the Lead reflector (yellow) and contained in a *2 cm* thick stainless steel vessel (green)[1].

[1] Is important to note that this figure represents only the starting point arrangement for the study of optimization of the reactor core and is not, therefore, the chosen configuration (which is the one shown in Figure 2.4) where the extension of the reflector and the total number of *FAs* will be optimized.

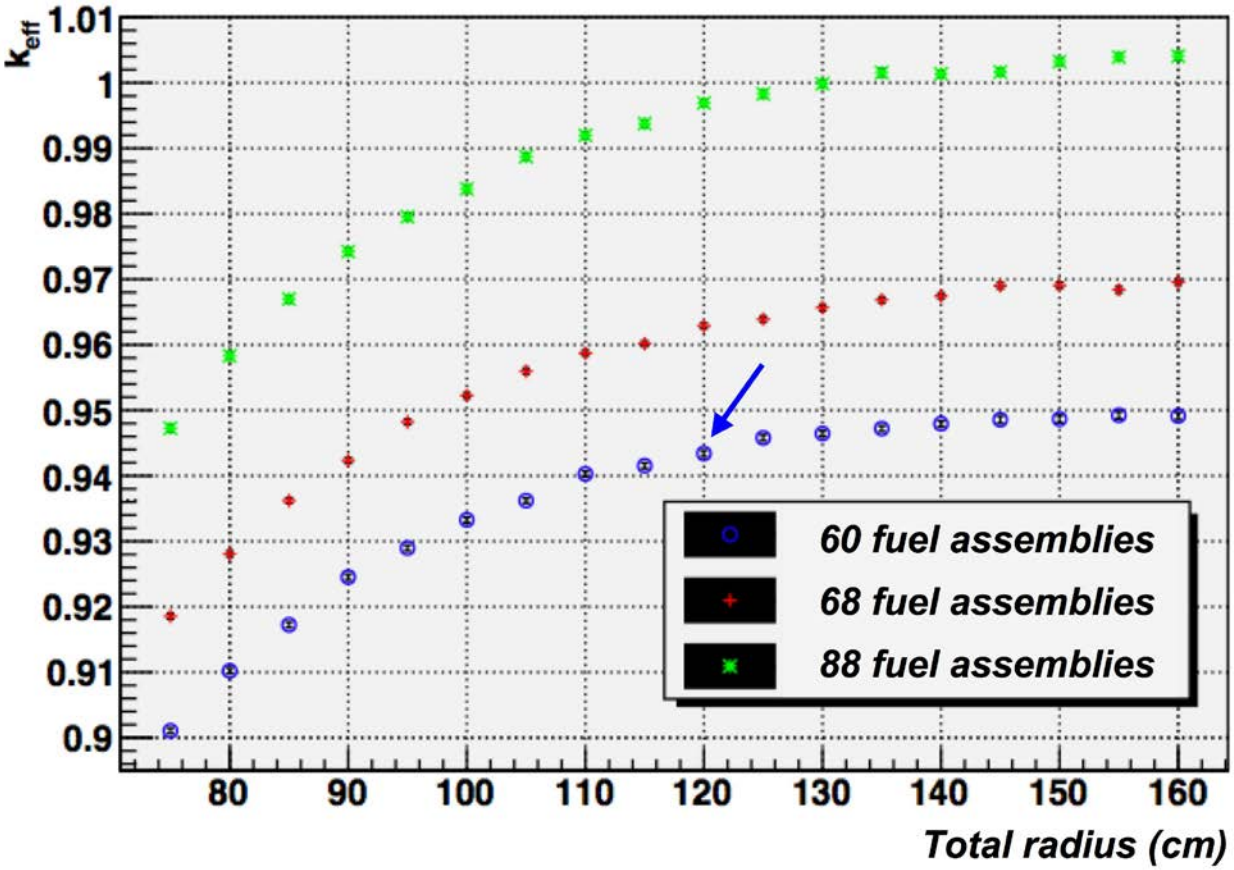

Figure 2.3 *FAs* number and total radius "balance". The blue arrow point out the configuration chosen for further studies.

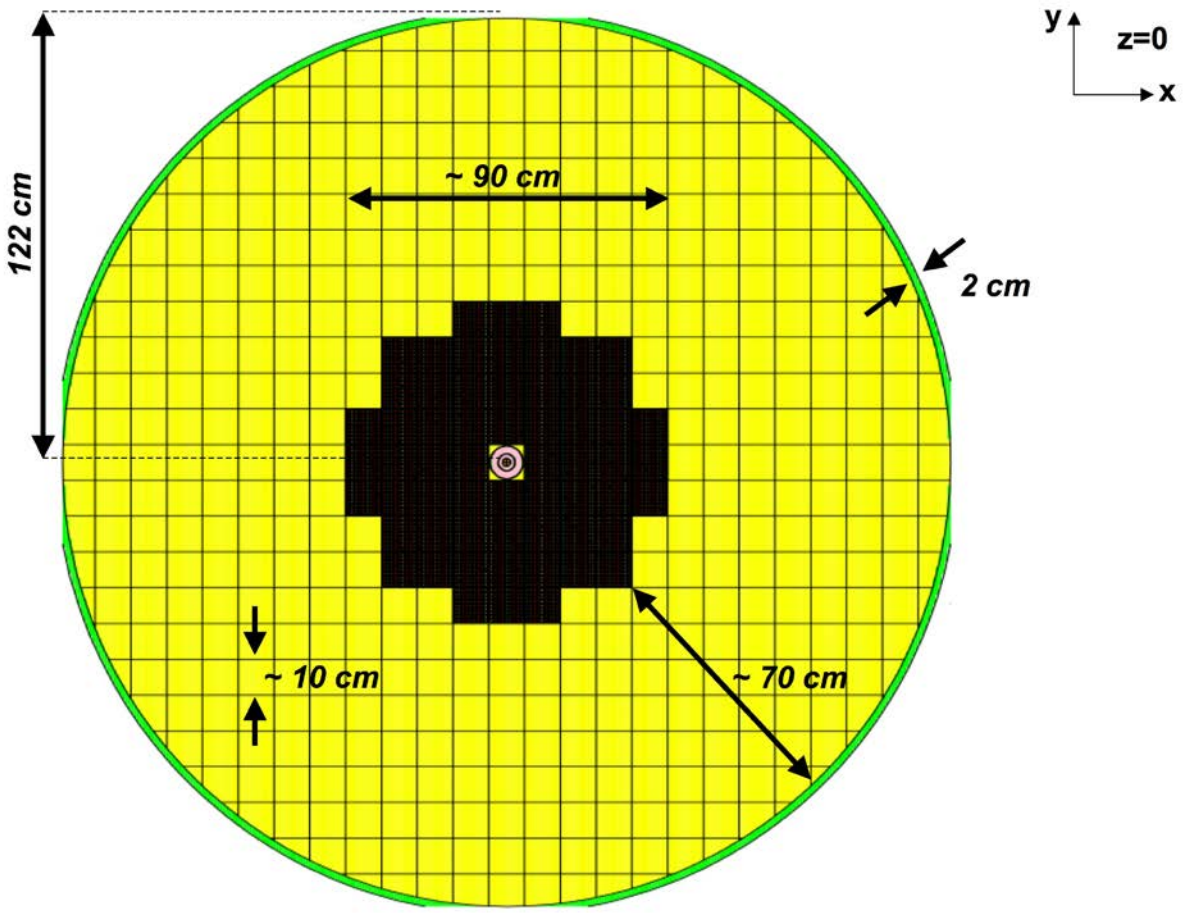

Figure 2.4 To-scale reactor cross-sectional area, now optimized.

The following table summarizes the different k_{eff} values that result from the use of different neutron cross-section data library in k-code simulations with *MCNPX* [2,3,4,5]; this table is important for the evaluation of a possible *systematic error* on k_{eff}. As shown, four different neutron cross-section data library were tested, including an old one, JENDL-3.2, whose result significantly differs from the mean value. However, this result has not been discarded, since more recent JENDL libraries directly in ACE format were not available at the time of this work.

Library	k_{eff}	σ	Year of publication
ENDF/B-VI	0.94559	0.00041	2001
ENDF/B-VII	0.94430	0.00045	2006
JEFF-3.1.1	0.94436	0.00044	2009
JENDL-3.2	0.95157	0.00046	1995

In the light of the simulations made, it was possible to estimate the mean value and the total error (systematic solely) on k_{eff}:

$$k_{eff} = \left(0.946 \begin{matrix} +0.007 \\ -0.003 \end{matrix} \right)$$

2.2 Beryllium Target Optimization.

After the optimization of reactor geometry, a study on the Beryllium target and on the "source term" was carried out. Figure 2.5 reports the transverse view of the target (TRADE conceptual design [6], see the paper "Target profile optimization" by M. Ciotti in this Focus Point).
The physical dimensions of the target, total radius *(2 cm)* and total height *(29.55 cm)*, are indicated in the figure, where *X* and *Z* are coordinates linked together by the following mathematical relation $Z_{(x)}=20 \cdot X-9.5$ for geometrical-structural reasons. The graph in this figure shows the fraction of proton leakage as a function of the crossed thickness *Z*. The blue arrow indicates the value to be used and this proposed size corresponds to *Z=3.0 cm (X=0.625 cm)*, a value comparable to the range of *70 MeV* protons in Beryllium [7]. Beyond this dimension, only secondary protons are lost whilst primary protons are completely stopped in the target; then increasing the dimension further is not useful. The chosen configuration minimizes proton leakage, size of the target and its cost.

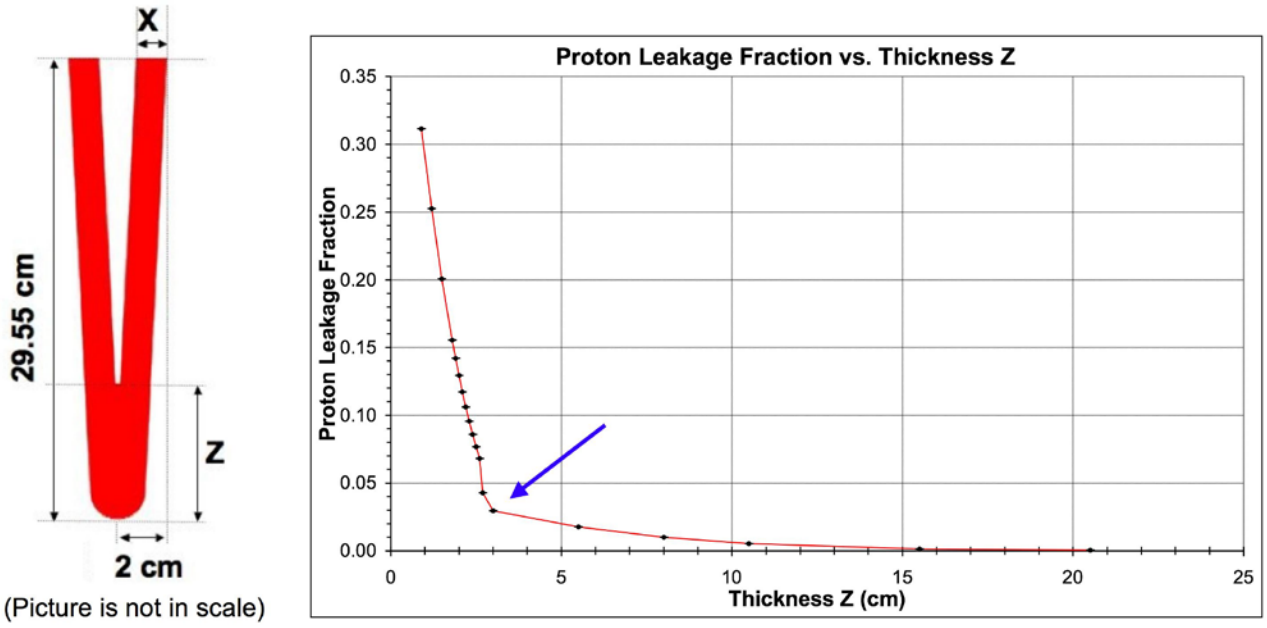

Figure 2.5 Target vertical-sectional area together with the graph of the proton leakage fraction vs. thickness "Z". The proposed size is marked with the blue arrow.

Once fixed the target size, the extension of the beam spot has been studied: in Figure 2.6 the fraction of proton leakage is plotted as a function of the beam spot radius *r*, assumed of circular shape in first approximation. Due to the particular target shape, the curve has an absolute minimum with increasing radius, before diverging when primary protons escape again. The configuration chosen minimizes proton leakage meanwhile maximizing the size of the beam, so that the power is deposited on a larger target volume, improving cooling.
After resizing the target and the beam spot, the source term has been characterized. The total neutron yield for incident proton is estimated by *MCNPX* to be about *0.091*, giving an absolute value of $4.3 \cdot 10^{14}$ neutrons coming out the target every second, if a proton source such as that described above is used. For completeness, the energy differential spectrum and the angular differential spectrum of the neutron source are shown in Figure 2.7. The fraction of forward

directed neutrons is equal to *73%*, while the fraction of "fast" neutrons (above *0.5 MeV*, which is the mean fission threshold energy of *MA*) is about *93%* of the total neutron source.

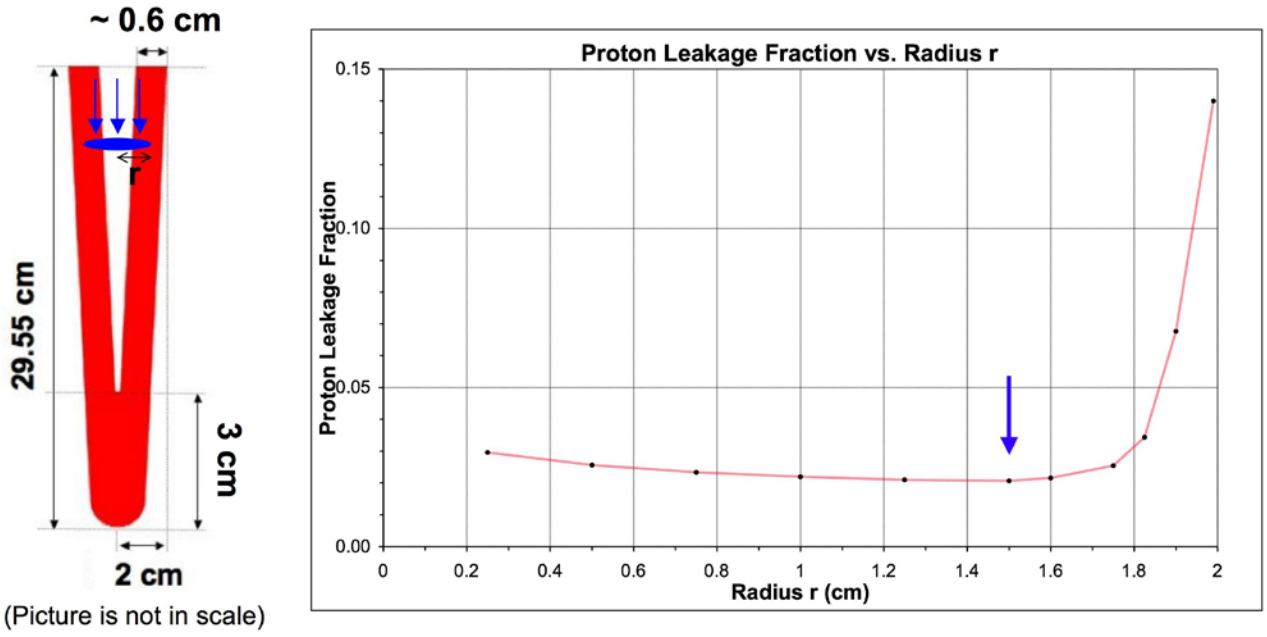

Figure 2.6 Proton leakage fraction vs. beam spot radius *"r"*. The proposed size is *r =1.5 cm*, corresponding to the absolute minimum of the curve.

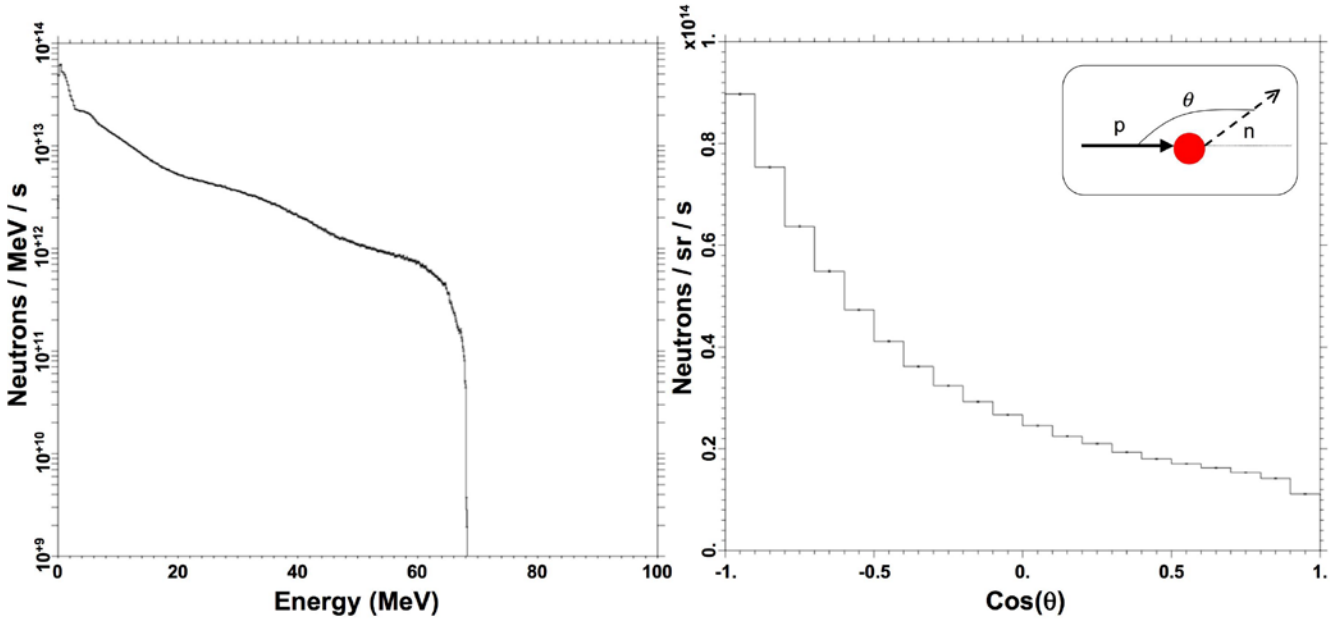

Figure 2.7 Neutron source energy (left) and angle (right) differential spectrum.

The profile of the power deposited in the target, shown in Figure 2.8, is fundamental for the design the target-dedicated cooling system: overall, the total power to be removed throughout the target is *49.3 kW*.

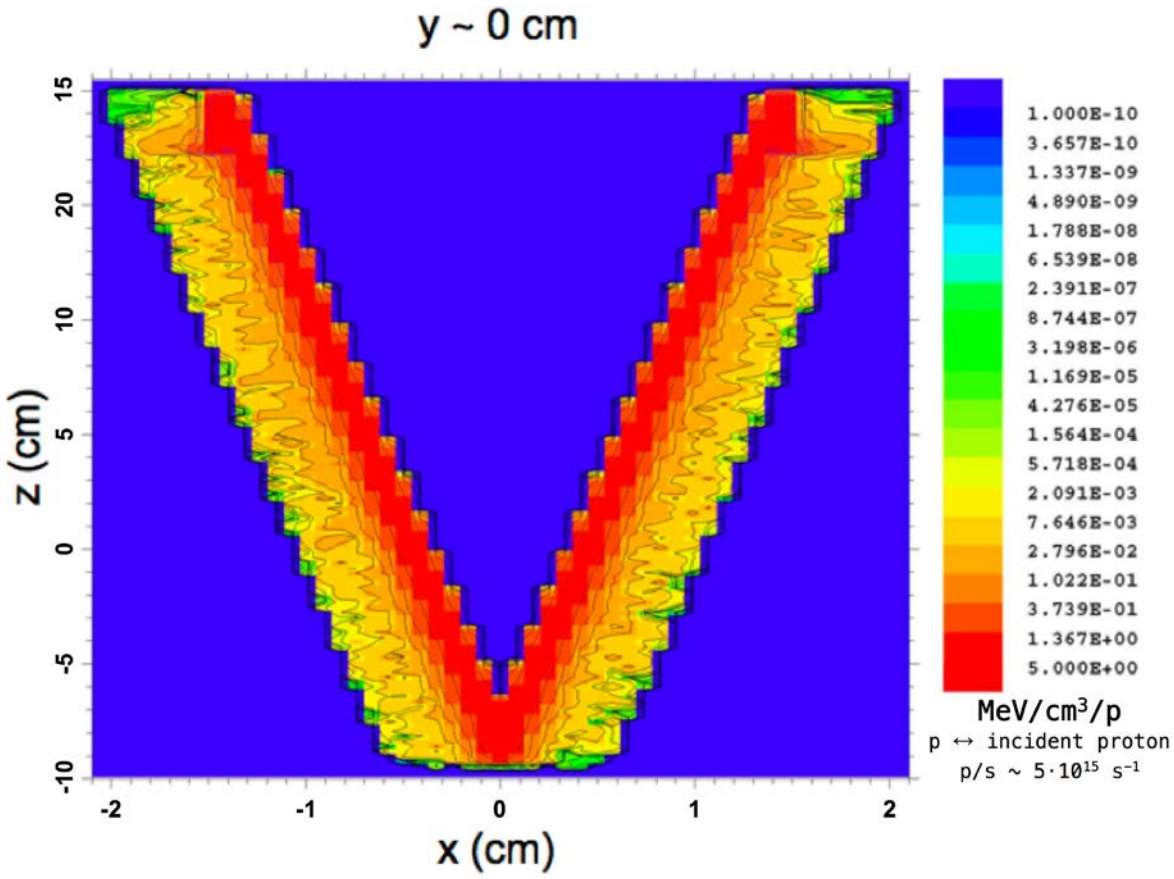

Figure 2.8 Power density deposited on the target volume, vertical-sectional area[2].

Last but not least, the target position along the reactor central axis has been optimized: with reference to Figure 2.9, the parameter δ, which is the distance between the midst of the active zone (blue dot) and the midst of the target (red dot) has been varied. As shown in Figure 2.10, $\delta = 5\ cm$ maximizes the power curve of the reactor as a function of the axial position of the target, so that the minimum number of neutron source from the active region is lost (*i.e.*, maximizing k_s). The two central points are not coincident, due to the fact that the neutron source angular distribution is mostly directed forward, along the proton source flight line, as shown previously.

[2] It may be useful to remember that $1\ MeV/cm^3/p = 0.75\ kW/cm^3$.

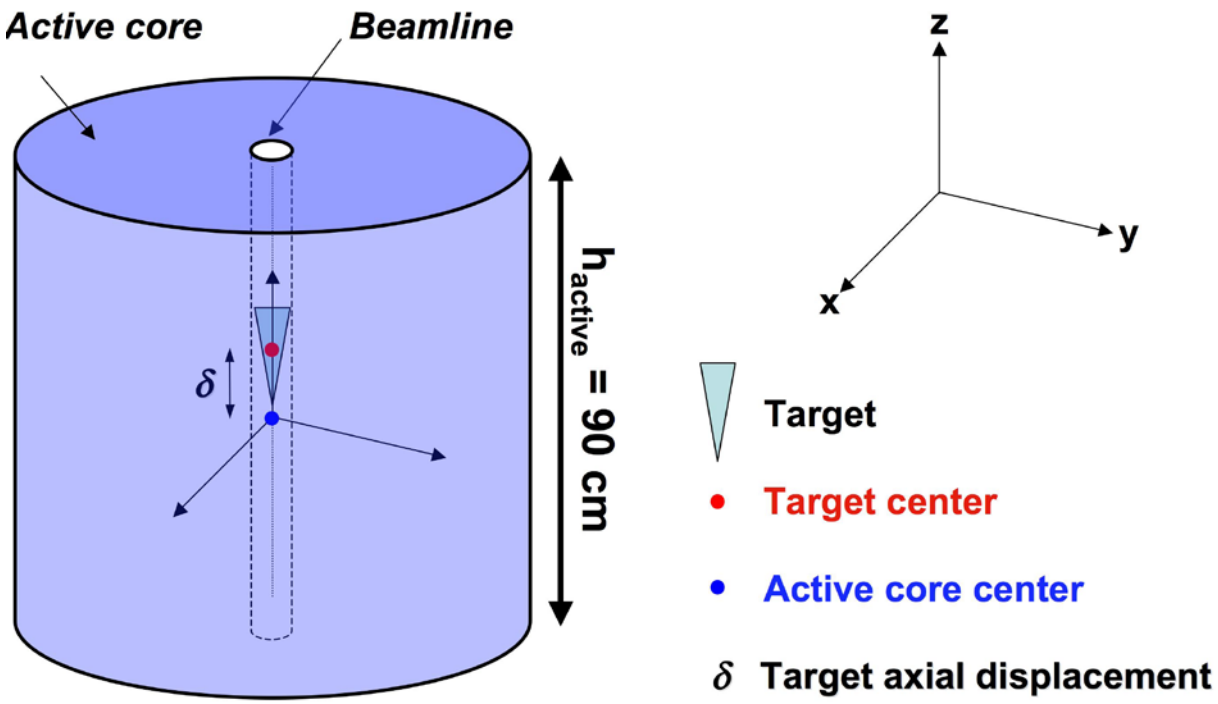

Figure 2.9 Sketch of the axial position of the Beryllium target in the reactor active core.

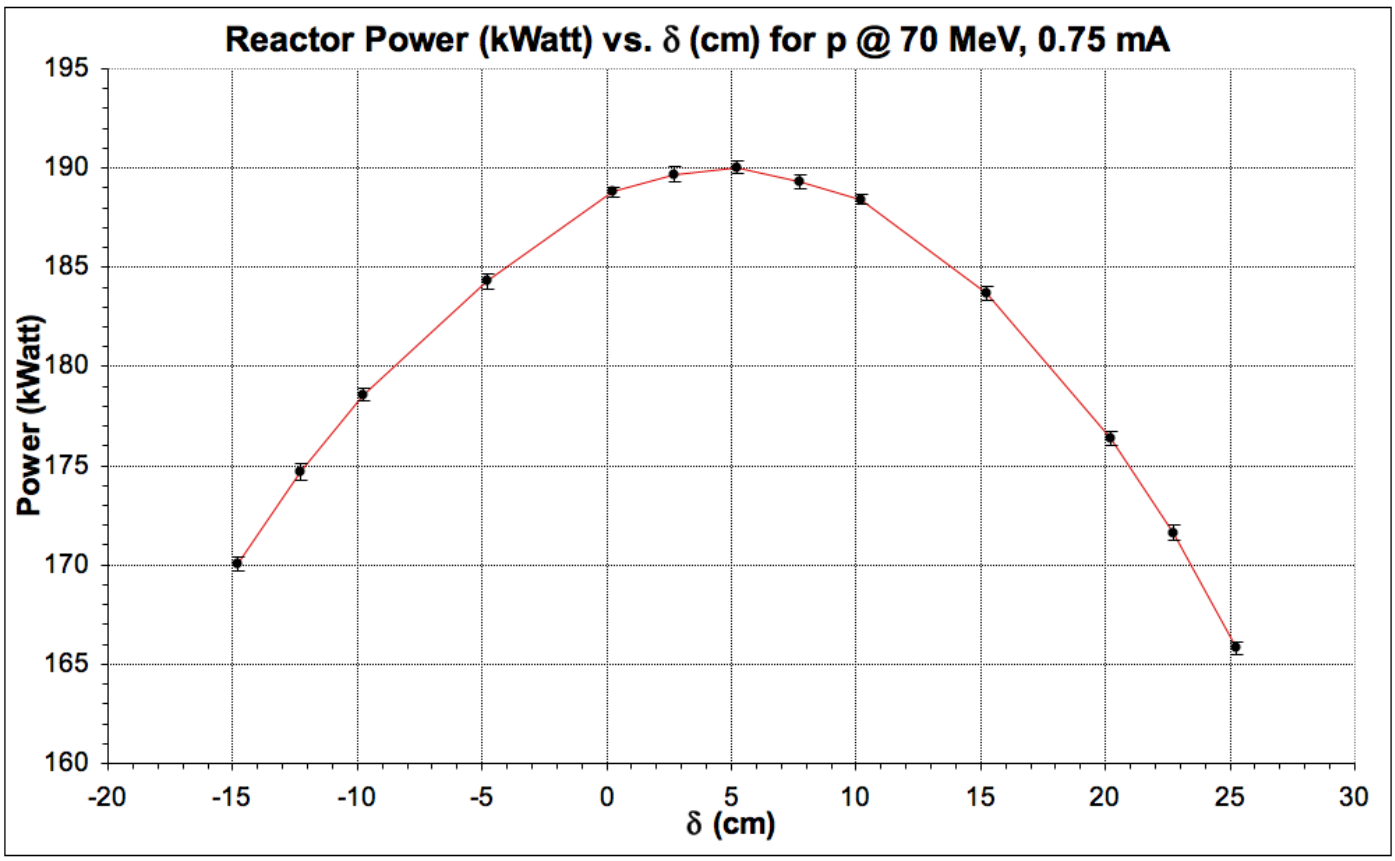

Figure 2.10 Reactor power vs. target axial displacement δ.

2.3 Thermal Power and Neutron Flux Simulations.

The total evaluated reactor power with its systematic error is P_{tot}=*(199+29-10)* kW_{th}, the mean value of each fuel rod is around *40 Watt* while the maximum is, for the inner rod which is closest to the source, *60 Watt*. The evolution of the thermal power of fuel rods in the radial direction is shown in Figure 2.11: this decreasing linear trend is typical of A.D.S. reactors with constant concentration of fuel, while at the end is well visible the contribution of the Lead reflector. The linear power density distribution along the axial direction in the inner rod (light blue) and in the outer one (red) is shown in Figure 2.12. It is evident that, while the distribution is practically symmetric around *0 cm* for the outer fuel rod, this isn't the same for the inner one, affected by the greater source contribution. These last two graphs are useful for sizing the reactor primary cooling system.

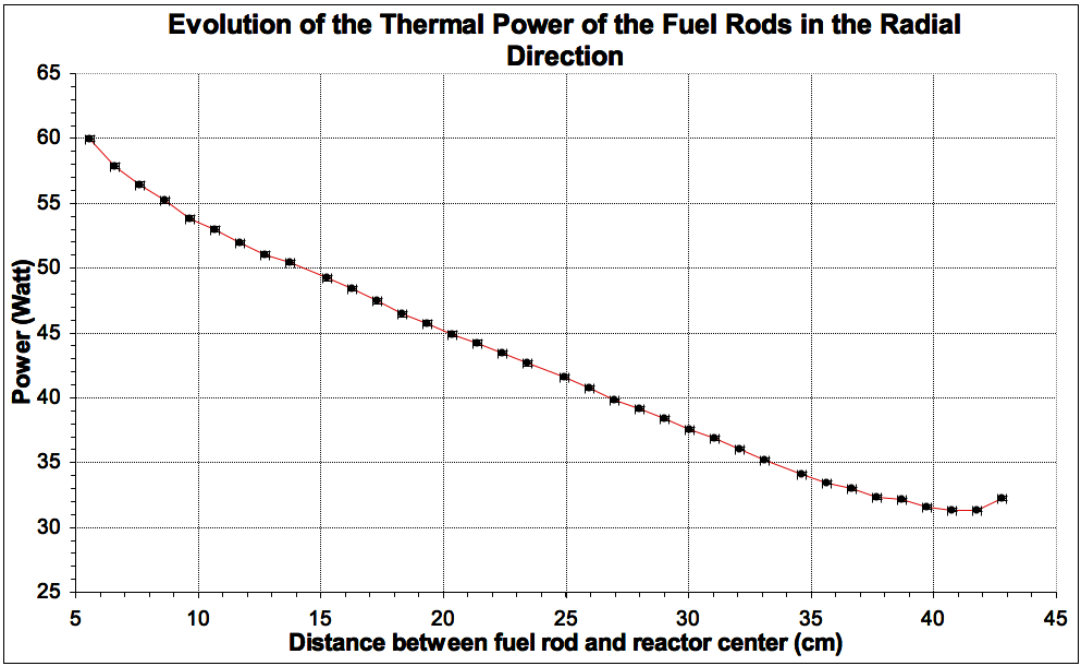

Figure 2.11 Spatial distribution of the thermal power of the fuel rods in the radial direction.

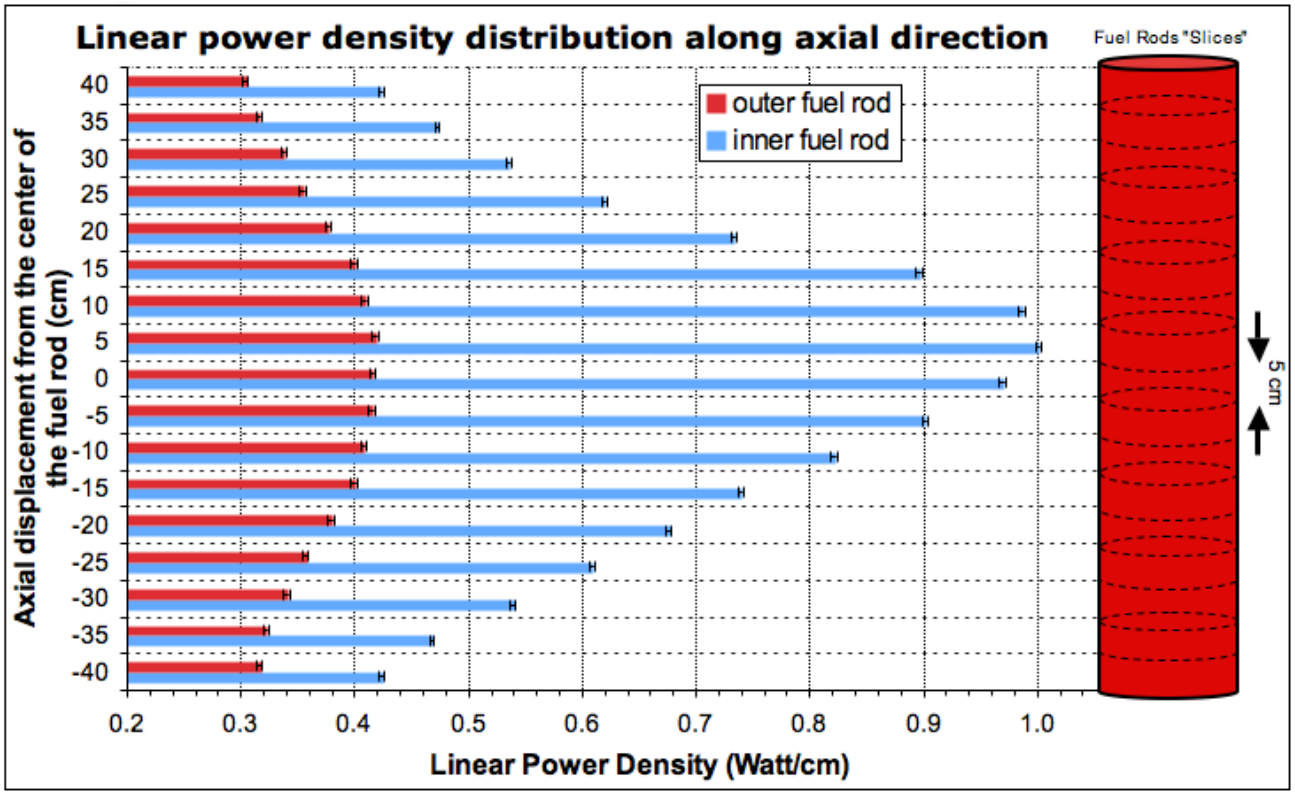

Figure 2.12 Linear power density distribution along the axial direction.

In Figure 2.13 is plotted the neutron flux spectrum in the inner fuel rod. For comparison, the fission cross-section of the most common Minor Actinides has been superimposed; this to emphasize the fast part of the spectrum useful for transmutation purposes. The integrated flux is around $6 \cdot 10^{12}$ $n/cm^2/s$ while the flux useful for fast fission, above *0.5 MeV*, amounts to *30%* of the integrated flux.
In Figure 2.14 the mean neutron flux in the reflector and the inner rod neutron flux are compared with the *radiative* capture (n, γ) cross-section: it is clear that the reflector region is more useful for the transmutation of radioactive isotopes of low atomic number: *i.e.* fission products. As order of magnitude, the integrated mean flux in the reflector is around 10^{12} $n/cm^2/s$.

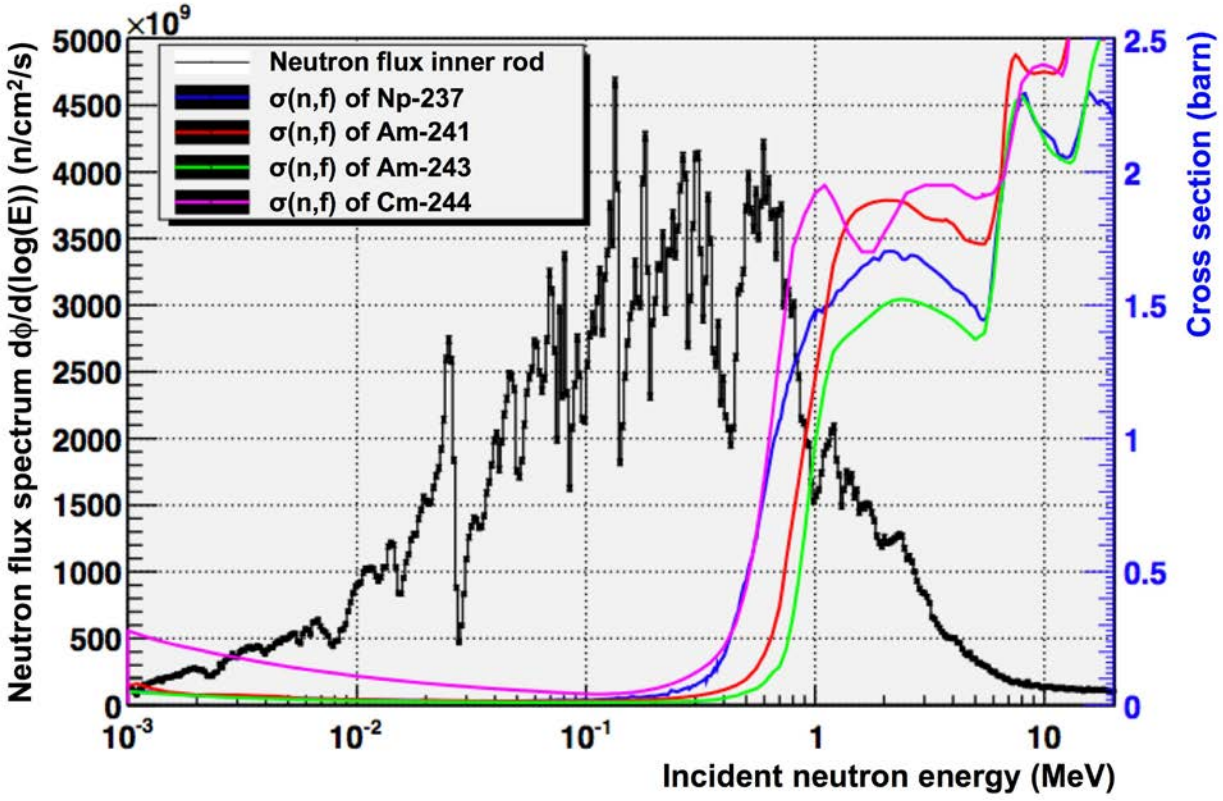

Figure 2.13 Inner rod neutron flux energy spectrum compared with the fission neutron cross-section in *MA*.

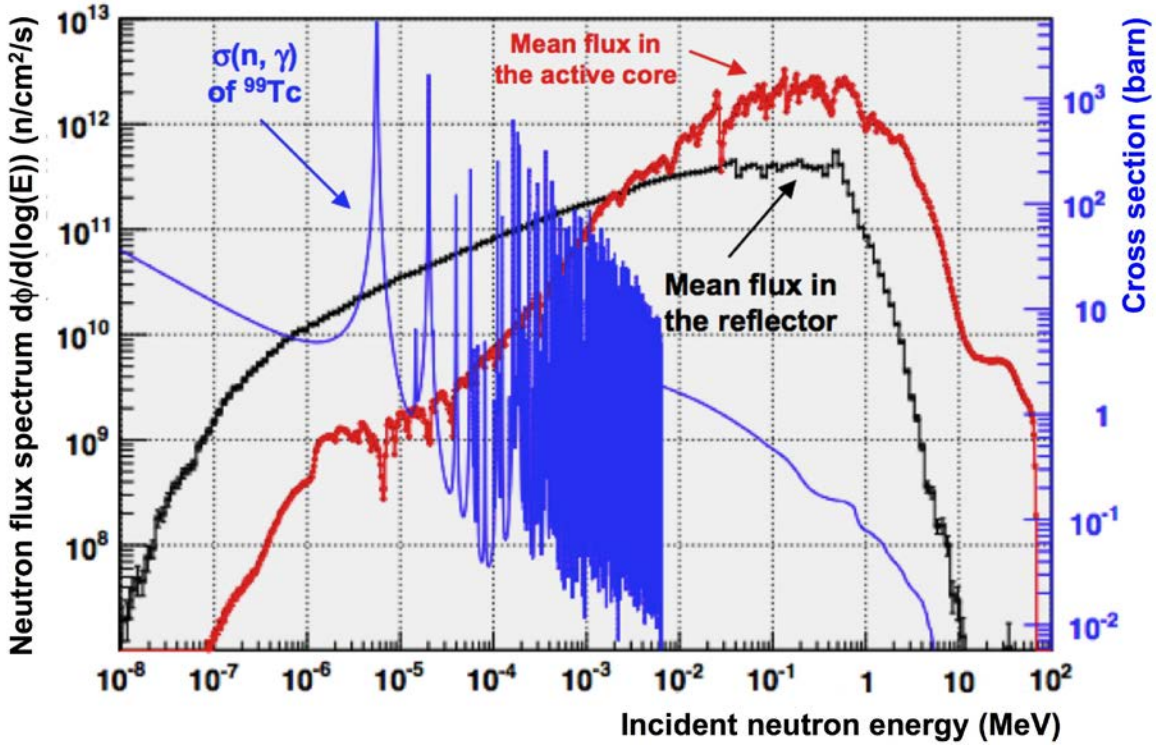

Figure 2.14 Average neutron flux in the reflector compared with the mean flux in the active core and the radiative capture cross-section.

2.4 Further evaluations.

2.4.1 Configurations with “holes”.

Since the reactor is proposed for personnel training and for research purposes, vacuum volumes placed inside the reactor, where to introduce any sort of nuclear instrumentation, are required. In this regard, different configurations can be designed, thanks to the “modular” concept of the active core and the Lead reflector. In this regard, a possible compromise can be given by an intermediate model where the configuration with “holes” and the “full” configuration have a k_{eff} slightly lower and slightly higher than *0.95* respectively (Figure 2.15). In this last case, the “full” configuration has k_{eff} just above specific; while the configuration with “holes” is the best one that preserves cylindrical symmetry with three voids in the active core, but unfortunately its k_{eff} is slightly lower than that required by the specifications. In this intermediate model, the total reactor power is around *300* kW_{th} and *160* kW_{th} for the “complete” configuration and the “holes” configuration respectively.

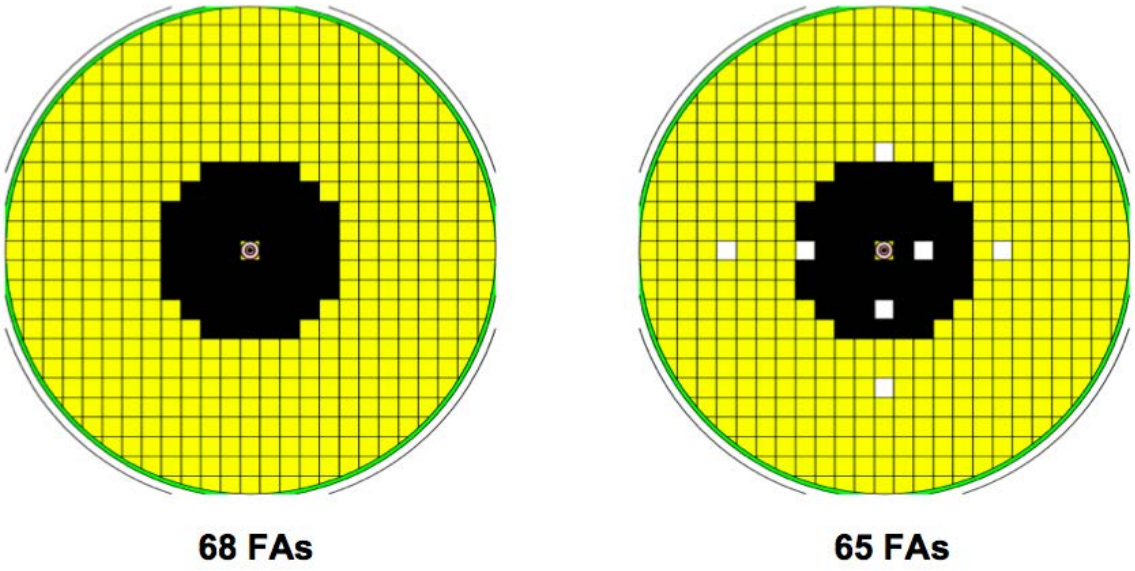

Figure 2.15 Intermediate model. Left: “full” configuration *(k_{eff} ~0.96)*; right: configuration with “holes” *k_{eff}~0.93*.

Therefore, in a core with *68 FAs*, reactors with k_{eff} between *0.93* and *0.96* can be easily composed and this would be very useful for studies of criticality and kinetics.
For completeness, the neutron flux energy spectrum was evaluated in the inner void volume and no appreciable difference in the shape of the energy spectrum was found, but only a global scale factor.

2.4.2 Deuteron beam.

Several “exploratory” simulations were also carried out using a deuteron beam of variable energy. The maximum energy of the beam has been chosen such that the range of deuterons in Beryllium is less than or equal to *70 MeV* proton range, so it has not been necessary to change the shape of the target.
First of all, the neutron source yield has been studied: the number of neutrons emitted per incident

particle as a function of the incident particle energy is shown in Figure 2.16. It is evident that *70 MeV* protons are “equivalent” to *50 MeV* deuterons and that *70 MeV* protons and deuterons differ almost by a factor of *1.9*. Clearly, total thermal power and neutron fluxes will be rescaled by the same factor: this result was confirmed by simulations, where no significant difference in the neutron spectrum shape of the inner fuel rod, which is considered as “reference”, was found.

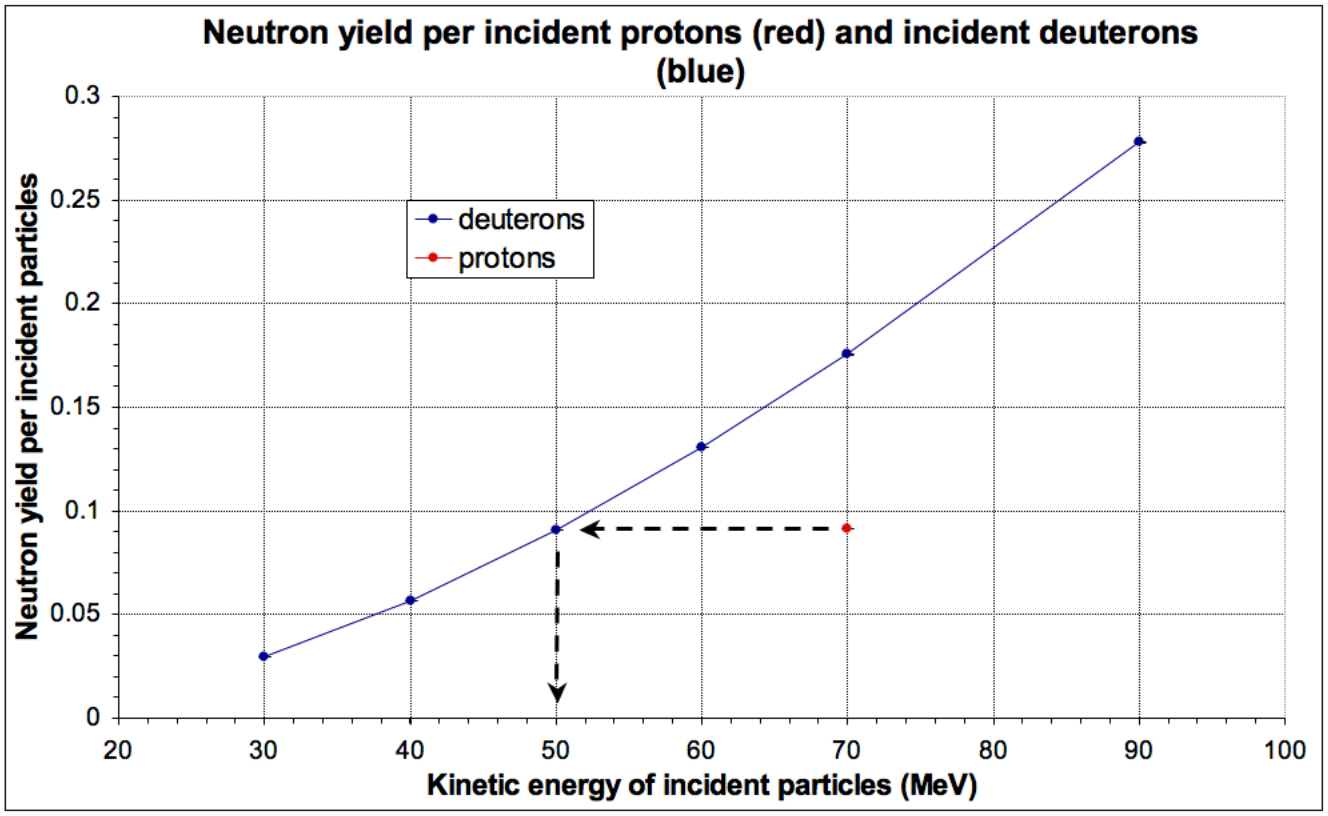

Figure 2.16 Neutron yield per incident proton (red) and deuteron (blue).

2.4.3 Tungsten target.

Preliminary simulations were performed with *70 MeV* protons and a target made of Tungsten: the target dimensions have been changed to take into account the different protons range in Tungsten. The results of the neutron source characterization are shown in the table below, in comparison with the ones obtained previously with the Beryllium target.

-	p @ *70 MeV* on Be	p @ *70 MeV* on W
Neutron yield Y_n^{tot}	$\approx 9.1 \cdot 10^{-2}$ n/p$_i$	$\approx 13.4 \cdot 10^{-2}$ n/p$_i$
"Fast" fraction neutron yield (≥0.5 MeV)	≈ 93.4%	≈ 81.9%
"Slow" fraction neutron yield (<0.5 MeV)	≈ 6.6%	≈ 18.1%

Although the neutron yield has slightly increased, neutron source energy spectrum has become quite "slower", as shown by the graph in Figure 2.17.

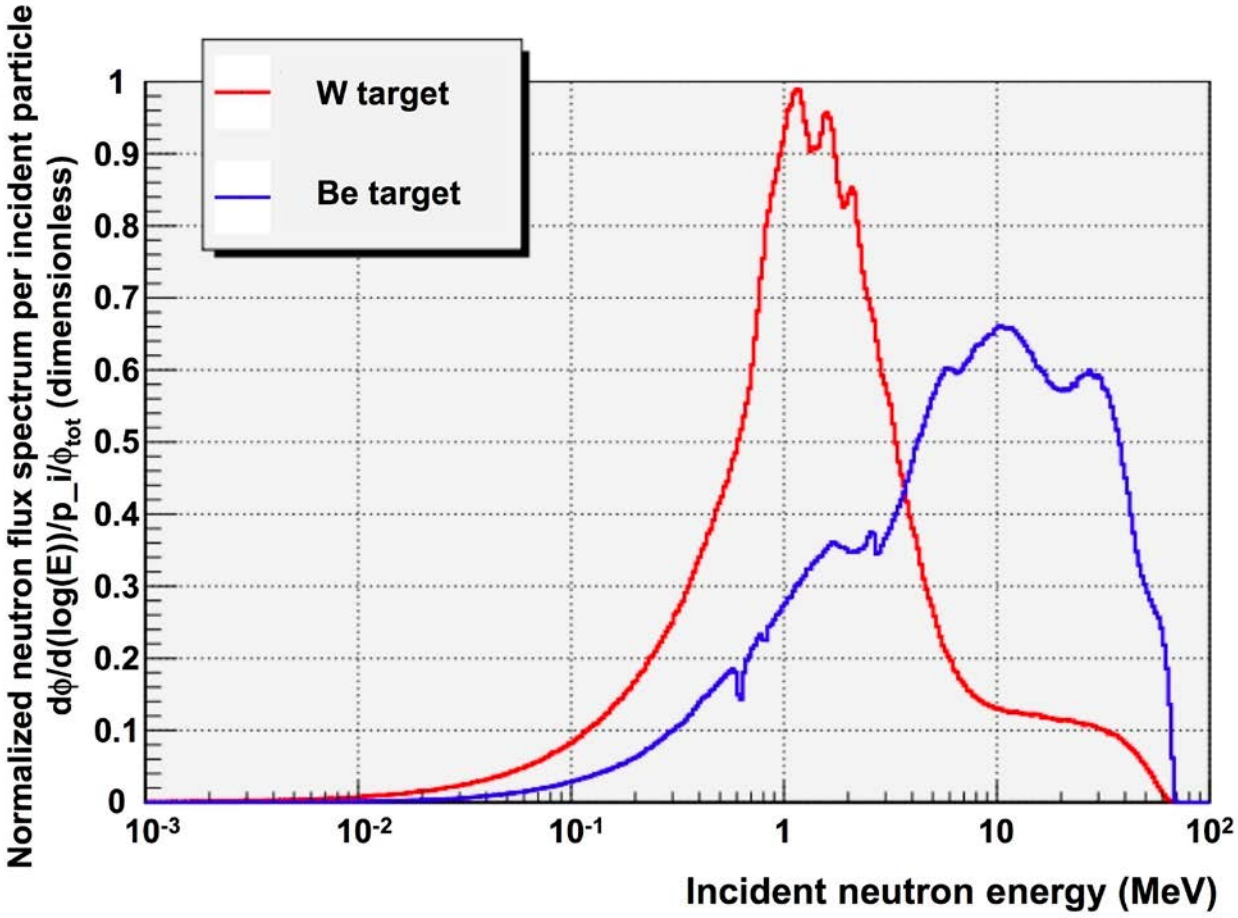

Figure 2.17 Neutron source energy spectrum using Be target (blue) and W target (red). Spectra are normalized for incident proton and for total neutron yield.

In addition, neutron source angular distribution is considerably more symmetrical than in the previous case with Beryllium target: it has been therefore necessary to study again the best axial position for the target, as done previously in Figure 2.10.
Following these optimization simulations, it has been assessed the thermal power of the reactor in this new configuration. Although the neutron yield is higher, the thermal power results *4%* lower than that obtained in the configuration with Beryllium target: this is probably due to the fact that neutrons from Beryllium are faster and make reactions *(n, 2n)* on Lead[3] with a reaction-rate greater than in the case of neutrons from Tungsten.

References

1. Pelowitz D. B., *MCNPX User's Manual, Version 2.6.0,* Los Alamos National Laboratory report **LA-CP-07-1473** (2008).

[3] Threshold at about *7.5 MeV*.

2. Chadwick M. B., Obložinský P. *et al.*, *ENDF/B-VII.0: Next Generation Evaluated Nuclear Data Library for Nuclear Science and Technology*, Nuclear Data Sheets **107** 2931-3060 (2006), http://www.nndc.bnl.gov/exfor/endf00.jsp .
3. ENDF/B-VI available at: http://www.nndc.bnl.gov/exfor/endf.htm (USA, 2001).
4. Santamarina A. *et al.*, *The JEFF-3.1.1. Nuclear Data Library: Validation Results from JEF-2.2 to JEFF- 3.1.1*, JEFF Report **22**, OECD/Nuclear Energy Agency (2009), http://www.nea.fr/dbforms/data/eva/evatapes/jeff_31/index-JEFF3.1.1.html .
5. Shibata K., Kawano T. *et al.*, *Japanese Evaluated Nuclear Data Library Version 3 Revision-2: JENDL-3.2*, Journal of Nuclear Science and Technology **32** 1259-1271 (1995), http://www.journalarchive.jst.go.jp/jnlpdf.php?cdjournal= jnst1964&cdvol=32&noissue=12&startpage=1259&lang=ja&from=jnlabstract.
6. Kadi Y. (CERN), *Spallation Target R&D for the EU Accelerator-Driven Sub-critical System Project*, conference hold at DESY Hamburg, Germany, (2004), http://www-mhf.desy.de/public/care04/2004.11.03_sr2/bene04_ykadi.pdf .
7. Berger M. J., Coursey J. S. *et al.*, *Stopping-Power and Range Tables for Electrons, Protons and Helium Ions*, National Institute of Standards and Technology Standard Reference Database **124** (2005), http://physics.nist.gov/PhysRefData/Star/Text/PSTAR.html .